ON-BOARD HEALTH ASSESSMENT OF AN ELECTRO-MECHANICAL ACTUATOR USING WAVELET FEATURES

J. Schaab†, M. Harrington‡ and U. Klingauf†
†Technische Universität Darmstadt, Institute of Flight Systems and Automatic Control,
Petersenstraße 30, 64287 Darmstadt, Germany
‡GE Aviation, Bishops Cleeve, Cheltenham, Gloucestershire GL52 8SF, UK

Abstract—To achieve condition-based maintenance, continuous on-board system monitoring is mandatory. Usage of additional sensors is restricted, as it would imply additional costs and sources of failure. In this paper the focus is on health assessment of an electro-mechanical actuator by monitoring the motor input current. A discrete wavelet transform is used to create features to distinguish different input current segments. Two modifications for derivation of enhanced wavelet features are described and their significance is evaluated. A pattern recognition step based on these features is realised through a bank of Support Vector Machines. This, together with an additional consolidation step provides information on the duration of the characteristic current segments as on certain events. Two fault states of the system can be detected and quantified based on the derived system information. This is shown by a measurement series with induced degradation of the actuator.

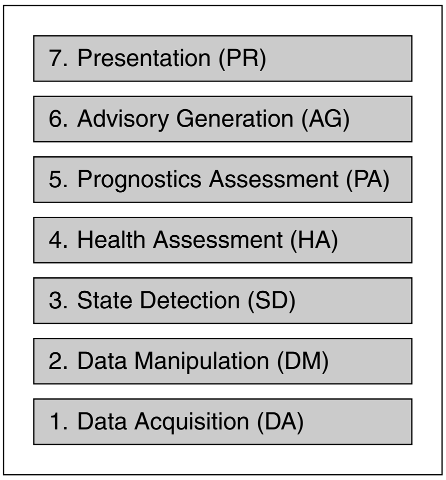

FIG. 1: Layers of the OSA-CBM model

1 INTRODUCTION

To maximise aircraft availability the time spent maintaining the aircraft must be reduced. Increased aircraft availability allows the operator, to improve return on investment in aircraft by improved utilisation. Maintenance can be reduced by either obviating the need for maintenance or reducing the time to undertake maintenance actions. The need for maintenance can be reduced by avoiding replacement of limited life components and instead replace components based on their condition. Alternatively or additionally through improved accuracy in diagnosis the time to repair failed systems can be reduced because the faulty component is quickly identified.

The *Technologies and Techniques for New Maintenance Concepts* (TATEM) project aims to provide the techniques to reduce the maintenance element of direct operating costs by 20 % in 5 to 10 years and 50 % in 10 to 15 years. The TATEM integrated project is part of the *Sixth Framework Programme* of the European Union. The TATEM project is striving to achieve these cost reductions by converting unscheduled maintenance to scheduled maintenance and improving the efficiency and effectiveness of maintenance actions. The work reported in this paper uses signal processing techniques to convert measured data into information about the health of a normal uplock actuator component.

The on-board condition assessment of actuators is part of an aircraft's health management system, which is part of the operator's health management system. One objective of condition monitoring is to translate a number of physical measurements into recommended maintenance action. The health management system monitors a multitude of information and forms a view of the aircraft's health, and then recommends maintenance action. Coalescing information from multiple sensors and sub-systems allows a holistic view to be taken and if implemented carefully avoid misleading diagnosis or incorrect recommendation of maintenance action. The *Open Systems Architecture for Condition-Based Maintenance* (OSA-CBM) [10] provides a layered framework and a definition of interfaces for health management systems, and has been adopted by the TATEM project. The layers of the OSA-CBM framework are illustrated in Fig. 1. The maintenance action recommendation results from the *Advisory Generation* (AG). The physical measurements are inputs to the *Data Acquisition* (DA) layer. In the progression from the DA through to the AG layer data is translated to knowledge and information useful to the operator.

This paper addresses in particular the data management, state detection and health assessment parts of the OSA-CBM framework and has used a Normal Uplock Actuator (NUA) as the candidate component.

2 NORMAL UPLOCK ACTUATOR

An aircraft is fitted with a number of uplocks, depending upon aircraft design. An uplock is used to hold landing gear or landing gear doors in place. To extend or retract the landing gear, the locks that hold landing gear & doors in place have to be released by a normal uplock actuator at the appropriate moment in the extension or retraction sequence. The uplock has proximity sensors to indicate the state of the lock. The Normal Uplock Actuator is part of an uplock. The Normal Uplock Actuator is powered from 28 V DC, and contains an electric motor with a retractable hook linking to the mechanics of the uplock. In normal operation the weight of the gear resting on the lock is removed by the extension and retraction sequencing before the Normal Uplock Actuator operates. The NUA incorporates EMI filtering, at the electrical connector input, to resist the effects of unshielded and untwisted aircraft wiring. It should be noted that EMI filtering can suppress signal components useful in health management. The Failure Modes and Effects Analysis indicate that electrical faults are more probable than mechanical faults.

The application of health management techniques to the normal uplock actuator should reduce the time to diagnose faults, thus reducing maintenance time. Ideally a forward looking prognosis giving an indication of an incipient failure would be beneficial, allowing for scheduled maintenance, instead of unscheduled maintenance on failure. The Normal Uplock Actuator was chosen for this work because of availability of a test item that could be degraded. The signals sensed to control operation of the NUA are the electrical current and voltage for the normal uplock actuator and for the uplock there are proximity sensors. Additional sensors give further information about the uplock operation but have a deleterious effect upon the uplock actuators reliability, thus only existing sensors are utilised if possible. The available design information of the NUA was limited. Hence, a model-based approach for system diagnosis could not be considered in this work. The proposed health assessment scheme is therefore based solely on analysis of the motor input current signal.

The NUA test rig provides the capabilities of simulating two fault conditions. System degradation by increased internal friction is the first considered fault. By application of an abnormal side load on the NUA slider mechanism is becomes possible to simulate the effect of increased friction. The second fault condition includes a degradation of the NUA motor efficiency. This is induced by insertion of an adjustable shunt resistance in one motor winding. This weakens the magnetic field and degrades the motor slightly up to a short circuit status. In this work the occurrence of only one fault at a time is considered.

The analysed input current signal of the NUA is shown in Fig. 2. There exits several operational phases during the unlock process of the system. These phases are reflected in the input current. Before initiation of the unlock process the system is *Idle*. After a short inrush transient the system is constantly moving and releasing the lock mechanism. In this phase *Move* the current signal is stationary. Then, after reaching the mechanical end stop, a second *Transient* phase occurs before the system enters again a stationary *Stall* phase. Shortly after 0.25 s and at 0.3 s some temporary *Spikes* can be observed. These spike events, together

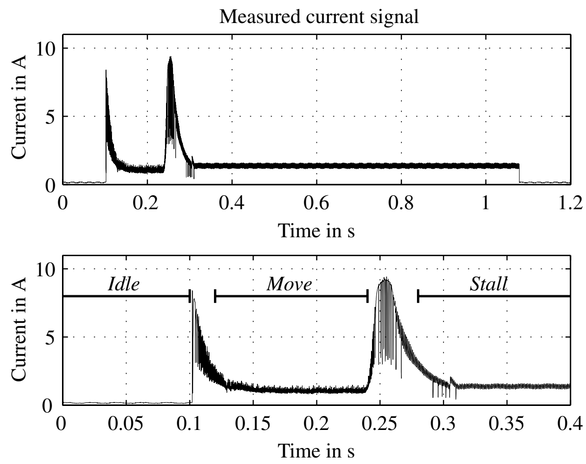

FIG. 2: NUA current signal and phase definition

with the defined signal phases, are later object of the applied pattern recognition system which is part of the NUA health assessment scheme.

3 SIGNAL TRANSFORMATION

For health assessment of the NUA it is necessary to derive features which describe the actual state of the system. Available noisy signals do not directly provide such features. In general a signal transformation is used to highlight features which are less distinct visible in the original signal. For the considered system a closer look at the frequency content of the signal could lead to valuable features.

In this section, we briefly describe the later used Wavelet transform (WT) and discuss the main differences in comparison to the Fourier transform (FT).

3.1 Fourier Transform

The Fourier transformation is used to convert a signal $x(t)$ from time domain to frequency domain. As orthonormal basis, the sine and cosine functions are used. The Fourier transform is given by the following equation

$$X_{\mathrm{FT}}(f) = \int_{-\infty}^{+\infty} x(t) e^{-j2\pi f t} \mathrm{d}t. \tag{1}$$

Stationary signals $x(t)$ can be recreated with the inverse Fourier transform from their frequency representation $X_{\mathrm{FT}}(f)$. This is not true for non-stationary signals, due to the missing time localisation of the used basis functions. A change in the frequency content of a signal over time can not be correctly seen in the transformed signal.

To overcome this drawback, the windowed Fourier transform or short-time Fourier transform (STFT) [2] was introduced, given by

$$X_{\mathrm{STFT}}(f,t) = \int_{-\infty}^{+\infty} x(t) w(\tau - t) e^{-j2\pi f \tau} \mathrm{d}\tau. \tag{2}$$

The window function $w(t)$, with window length T_N, which is non-zero only for $|t| \leq T_N/2$, is multiplied with the signal

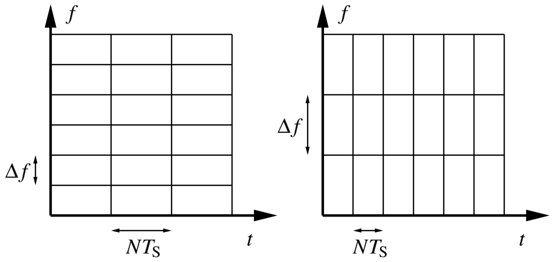

FIG. 3: STFT—segmentation of time-frequency plane

$x(t)$ before computation of the frequency content. Hence, only in the vicinity of the analysis point t the frequency content of $x(t)$ is evaluated in Eq. (2) and the desired time localisation is achieved. The choice of the window length T_N determines the obtained time resolution of the STFT. However, this determines the frequency resolution as well, which is reciprocal to the time resolution. This is a consequence of the uncertainty principle of signal analysis [2]. The STFT has a uniform segmentation of the time-frequency plane with fixed resolution. This is shown in Fig. 3 for two different window lengths.

Digital signal processing requires a discrete version of the Fourier transform. The discrete time signal $x(k) = kT_S$, $k = 0,1,\ldots,N-1$ with finite length N, is analysed at discrete frequencies $f(n) = n\Delta f$ where $\Delta f = 1/NT_\mathrm{S}$ and $n = 0,1,\ldots,N-1$. The discrete-time Fourier transform (DTFT) is

$$X_{\mathrm{DTFT}}(n) = \sum_{k=0}^{N-1} x(k)e^{-j\frac{2\pi n}{N}k}\ ,\ n = 0,1,\ldots,N-1. \tag{3}$$

The relationship between signal length N, or window length NT_S, and the obtained frequency resolution Δf is here clearly visible. To obtain a good frequency resolution, one has to choose a wide window, which, however, leads to poor time resolution and vice versa.

3.2 Wavelet Transform

The uniform segmentation of the STFT and its discrete implementation is not the best choice for all analysis situations. There are good reasons for choosing an non uniform segmentation. It could be valuable to have a good time resolution for high frequencies, for which the point in time when an event happens is more interesting than the exact frequency. For low frequencies however, one could be more interested in having a good measure for the actual frequency then the exact point in time when it occurred. The Wavelet analysis possesses such a non uniform segmentation of the time frequency plane and is an alternative way of signal analysis to the FT.

The basis function of the WT, the *wavelet*, is both localised in frequency and in time, whereas the basis function of the FT is only localised in frequency. Hence, no window function is needed in WT to analyse non-stationary signals. Any square integrable function which fulfils the admissibility condition [8] can be chosen as mother wavelet $\psi(t)$.

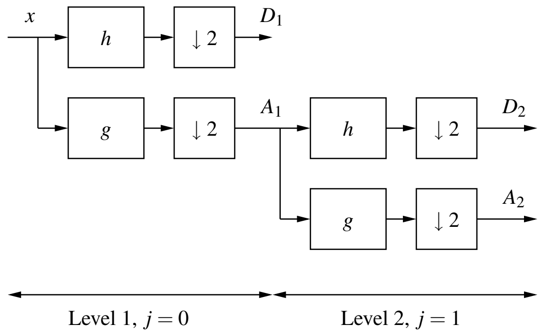

FIG. 4: Two level decomposition filter bank

The mother wavelet

$$\psi_{s,\tau}(t) = \frac{1}{\sqrt{s}}\psi(\frac{t-\tau}{s}), \tag{4}$$

is scaled by parameter s and translated by parameter τ. This forms a set of basis functions used for calculation of the wavelet coefficients in the Wavelet transform [4]

$$X_{\mathrm{CWT}}(t,s) = \frac{1}{\sqrt{s}}\int_{-\infty}^{+\infty} x(\tau)\psi(\frac{\tau-t}{s})\mathrm{d}\tau\ ,\ s,\tau \in \mathbb{R}. \tag{5}$$

Eq. 5 describes the continuous Wavelet transform (CWT), both parameters s and τ have continuous values. The relationship between scale s and frequency f is inverse proportional. For a practical computation, discrete values need to be chosen for these parameters. Even for discrete values a perfect reconstruction of $x(t)$ can be obtained under certain conditions, as the information contained in the coefficients of the CWT is highly redundant [3]. The redundant information in Eq. (5) is removed by choosing $s = 2^j, \tau = k2^j$ with $j,k \in \mathbb{N}_0$. The wavelet function is still continuous, only the analysis points are discrete in time and scale. This has removed redundancy, but now the obtained transform is no longer shift invariant, i.e. a shift of $x(t)$ is not a simple shift in $X(t,s)$. This needs to be considered in the derivation of wavelet features as discussed later.

There exists a strong relationship between this discretised WT and the concept of filter banks or multiresolution analysis [5] [9]. In multiresolution, a signal is simultaneously analysed at different scales, and filter banks provide a way to do this efficiently. A two channel filter bank, depicted in Fig. 4, consists of a high-pass filter h and a low-pass filter g applied in parallel to a signal. On each filter output a downsampling step $\downarrow$ with factor 2 is applied to make the overall signal length after the filter bank equal to the length before. In applying the same filter bank repeatedly on the output of the low-pass filter, a multiresolution analysis is performed which provides a computational efficient way for calculation of a discretised WT [5]. For each level j the wavelet, or *detail coefficients* D_{j+1}, representing scale 2^j are obtained as the output of the high-pass filter after downsampling. Looking at the structure of the filter bank, the segmentation of underlying time-frequency plane becomes clear. The detail coefficients D_1 contain the high frequency parts and are updated frequently, while the coefficients of the subsequent levels contain lower frequency

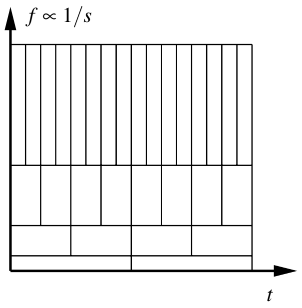

FIG. 5: WT—segmentation of time-frequency plane

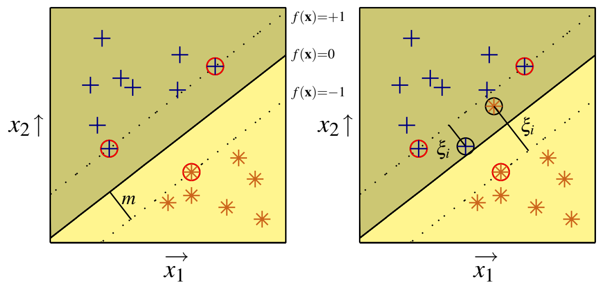

FIG. 6: SVC—separable and non-separable classes

components and are updated at half the rate of the previous level. In Fig. 5 the segmentation of the time-frequency plane of the discrete Wavelet transform is shown. Here, the non-uniform segmentation becomes visible, which has the properties discussed in the beginning of this subsection.

4 SUPPORT VECTOR CLASSIFICATION

The goal of classification is to find a correlation between features derived from items of given classes and their belonging class labels. This correlation is expressed in a decision function which is used by a pattern recognition system for correct identification of unseen items. Support Vector Machines (SVMs) [11] provide an elegant way for calculating a decision function based on a given training data set, which is optimal in a certain way. The fundamentals of Support Vector Classification (SVC) are summarised in this section.

4.1 Linear separable classes

The principle of Support Vector Classification is best studied for the most simple case—where the classes are linear separable. All classification problems can be reduced to a digital case, where the classifier is designed to distinguish between two classes, with class label $y = +1$ or $y = -1$. The training dataset, with feature vector $\mathbf{x}_i$, is given by

$$\text{(6)} \qquad \{(\mathbf{x}_i, y_i)\}_{i=1}^{N}, \quad \mathbf{x}_i \in \mathbb{R}^n, \quad y_i \in \{-1, +1\}.$$

The required classifier is here a linear decision function

$$\text{(7)} \qquad f(\mathbf{x}) = \mathbf{w}^{\mathrm{T}}\mathbf{x} + b,$$

with coefficient vector $\mathbf{w}$ and scalar bias term b. A proper decision function $f(\mathbf{x}_i)$ gives a positive value for $y_i = +1$ and negative values for $y_i = -1$. The class boundary—or separating hyperplane—is found for $f(\mathbf{x}) = 0$. For a linear separable training dataset, the requested properties do not specify a unique decision function. Hence, a further requirement is used to remove this ambiguity. The data points $\mathbf{x}_i$ which are nearest to the separating hyperplane have to fulfil $|f(\mathbf{x}_i)| = 1$. This does not only define a unique decision function, but also implies a class boundary which has maximum distance to the data points. The margin m between the separating hyperplane and the nearest data points can now be expressed as $m = 1/||\mathbf{w}||$. This leads to the primal optimisation problem for linear SVC [7]

$$\text{(8a)} \qquad \min_{\mathbf{w}} \quad J_{\mathrm{p}}(\mathbf{w}) = \frac{1}{2} \parallel \mathbf{w} \parallel^2$$

$$\text{(8b)} \qquad \text{s.t.} \quad y_i(\mathbf{w}^{\mathrm{T}}\mathbf{x}_i + b) \geq 1 \quad \forall \quad i = 1, \ldots, N.$$

The object function $J_{\mathrm{p}}(\mathbf{w})$, which is to be minimised, describes the desired maximum margin, while the constraint reflects the correct behaviour of the decision function and includes the normalising property described above. In the left graph of Fig. 6 the separating hyperplane is given as a solid line together with the maximum margin as dashed lines. Any other choice of the linear class boundary would result in a smaller margin. This explains the good generalisation abilities of SVC. As a result of the maximised margin the obtained classifier gives the best separation of the two classes based on the given training data [11].

4.2 Linear non-separable classes

The limitation to fully separable classes prevents application to most real world cases. Therefore, the optimisation problem needs to be extended in order to deal with non-separable classes. This is achieved by introduction of positive slack variables $\xi_i \geq 0$ which describe an excess of a data point beyond the margin, exemplary shown in the right part of Fig. 6. With these slack variables, it becomes possible to weaken the constraint in Eq. 8b which otherwise can not be fulfilled for overlapping classes. However, weakening this constraint alone is not sufficient, as the constraint would be always satisfied. Hence, this has to be considered in the objective function by introducing the sum of all slack variables to be minimised as well. This gives the *primal* optimisation problem of linear SVC for non-separable classes

$$\text{(9a)} \qquad \min_{\mathbf{w},\xi} \quad J_{\mathrm{p}}(\mathbf{w}, \xi_i) = \frac{1}{2} \parallel \mathbf{w} \parallel^2 + C \sum_{i=1}^{N} \xi_i$$

$$\text{(9b)} \qquad \text{s.t.} \quad y_i(\mathbf{w}^{\mathrm{T}}\mathbf{x}_i + b) \geq 1 - \xi_i \quad \forall \quad i = 1, \ldots, N$$

$$\text{(9c)} \qquad \xi_i \geq 0 \quad \forall \quad i = 1, \ldots, N.$$

In Eq. 9a parameter C is introduced, which allows for trade-off between the margin width and number of outliers.

4.3 Dual formulation

To solve the optimisation problem in Eq. 9, its Lagrangian formulation is used. The resulting *dual* optimisation problem has a comfortable mathematical form; after introduction of dual variables α_i the problem can be written as a convex quadratic program [1]

$$\min_{\alpha} \quad J_{\mathrm{d}}(\alpha) = \frac{1}{2}\sum_{i=1}^{N}\sum_{j=1}^{N} \alpha_i\alpha_j\, y_i y_j\, \mathbf{x}_i^{\mathrm{T}}\mathbf{x}_j - \sum_{i=1}^{N}\alpha_i \tag{10a}$$

$$\text{s.t.} \quad 0 \le \alpha_i \le C \quad \forall \quad i = 1,\dots,N \tag{10b}$$

$$\sum_{i=1}^{N} \alpha_i\, y_i = 0. \tag{10c}$$

With the dual variables the decision function is expressed in *support vector* (SV) representation

$$f(\mathbf{x}) = \sum_{i=1}^{N} \alpha_i y_i\, \mathbf{x}_i^{\mathrm{T}}\mathbf{x}. \tag{11}$$

In Eq. 11 the meaning of a support vector becomes apparent. Those data points $\mathbf{x}_i$ whose dual variable α_i is non-zero are called support vectors. Only data points with a positive slack variable in the primal problem together with all points lying exactly on the margin end up as SV. In general this is only a small fraction of all data points. In Fig. 6 a circle marks the data points which remain as SVs.

4.4 Nonlinear SVC

So far, only linear decision functions are used as classifier. To extend this method to nonlinear problems, a nonlinear mapping ϕ of the input space to a higher dimensional feature space is applied [7]. In this feature space, the discussed linear SVM is directly applicable now working on the transformed data points $\phi(\mathbf{x})$. To avoid the direct formulation of this nonlinear mapping and to avoid the computation of a scalar product on a higher dimensional vector, the *kernel trick* is used. This becomes possible as in Eq. 10 and in decision function Eq. 11 the input data appears only in form of scalar products $\mathbf{x}_i^{\mathrm{T}}\mathbf{x}$. The kernel trick replaces these scalar products by a kernel function

$$k(\mathbf{x}_i,\mathbf{x}_j) = \phi(\mathbf{x}_i)^{\mathrm{T}}\phi(\mathbf{x}_j). \tag{12}$$

As kernel function e.g. a Gaussian function is valid, other possibilities can be found in [7]. The necessary conditions for a proper kernel function are given in [11]. The Gaussian function leads to very flexible classifiers and is used in the following.

With the definition of a kernel matrix $\mathbf{H}$, wherein $h_{ij} = k(\mathbf{x}_i,\mathbf{x}_j)$, the final optimisation problem is given in matrix form as

$$\min_{\mathbf{a}} \quad J_{\mathrm{d}}(\mathbf{a}) = \frac{1}{2}\mathbf{a}^{\mathrm{T}}\mathbf{H}\,\mathbf{a} - \mathbf{y}^{\mathrm{T}}\mathbf{a} \tag{13a}$$

$$\text{s.t.} \quad -C \le a_i \le C \quad \forall \quad i = 1,\dots,N \tag{13b}$$

$$a_i y_i \ge 0 \quad \forall \quad i = 1,\dots,N \tag{13c}$$

$$\sum_{i=1}^{N} a_i = 0, \tag{13d}$$

with the decision function

$$f(\mathbf{x}) = \sum_{i=1}^{N} a_i\, k(\mathbf{x}_i,\mathbf{x}) + b. \tag{14}$$

In this form, the dual variables α_i are replaced by SVM coefficients a_i as $a_i = \alpha_i y_i$ similar to the approach in [6] for SV regression.

The problem dimension of SVC is determined by the number of training data N. This requires special optimisation routines for solving the problem. However, the length of vector $\mathbf{x}$, i. e. the number of features, does not significantly complicate the procedure. Therefore, Support Vector Machines are well suited for large feature vectors. The proposed health assessment scheme takes advantage of this.

5 NUA HEALTH ASSESSMENT

This section describes the proposed health assessment scheme for the Normal Uplock Actuator. The procedure follows basically the process of health assessment as described by the OSA-CBM structure. The approach is now summarised and discussed in more detail in the following subsections.

The requirement of on-board diagnosis in only using available sensors, restricts the analysis of the NUA to the motor current signal. With this signal, the data manipulation step aims to transform the raw signal to a more appropriate representation for further analysis. Here, a discrete wavelet transformation using a filter bank is applied. A set of wavelet features is derived from the transformed signal. The chosen set of coefficients is optimised to allow reliable detection of the different operational phases of the NUA as discussed later. By using a bank of SVMs, these wavelet features are taken to estimate the NUA operational phases as well as defined events. This concludes the data manipulation step and leads over to the state detection step. Here, a few higher features are considered which allow detection of the state of the NUA. Two fault states are examined and classifiers are designed to identify each state properly. Based on the system state information the health assessment step can estimate the health of the NUA eventually. This step uses the higher features to derive a quantitative measure of the system health.

The complete health assessment scheme is now described in more detail.

5.1 Wavelet Features for Phase Detection

The health assessment of the NUA starts with the extraction of features from the available current signal. Here, a set of wavelet coefficients shall directly be used as input to classifiers for detection of the operational NUA phases. In the following, two different wavelet feature sets are considered. Apparently, to take just the actual output of the filter bank is the simplest choice as set of wavelet features. Later this is referred to as the *vertical slice* (VS) configuration. Instead of taking just the actual wavelet coefficients,

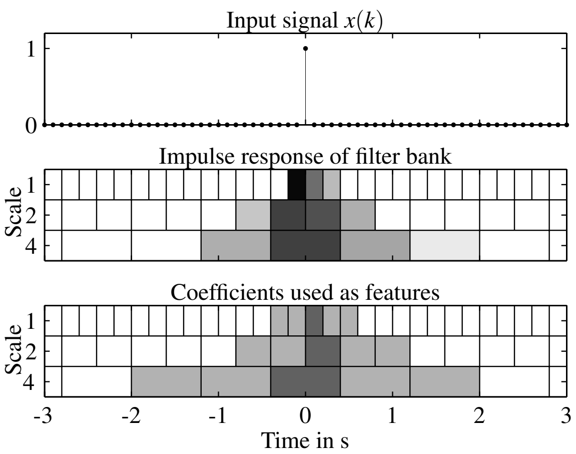

FIG. 7: Impulse response of filter bank and location of coefficients used as features

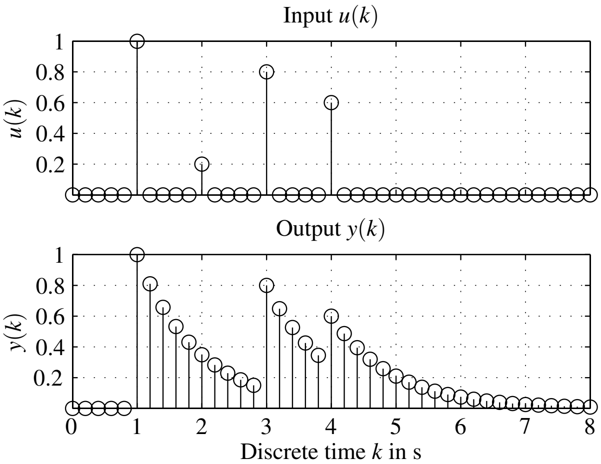

FIG. 8: Smoothing filter for wavelet coefficients

it might be valuable to include further coefficients from adjoining time points. The choice of adjoining wavelet coefficients is motivated by the form of the impulse response of the used filter bank. The impulse response of a three level *db3*-filter bank is shown in the middle graph of Fig. 7. The segments of non-zero wavelet coefficients are highlighted according to the absolute value of the coefficients. All non-zero coefficients form a pyramidal structure, where the number of non-zero segments per scale can vary according to a shift in the input signal. This is due to the missing shift invariance of the discrete Wavelet transformation. In the lower graph of Fig. 7 all highlighted coefficients form the *impulse pyramid* (IP) configuration (light and dark grey). This IP configuration captures more information compared to the VS configuration, which includes only the coefficients at current time (dark grey). The number of adjoining coefficients per scale is determined by the filter length n_f of the used FIR wavelet filter. For a given filter length $n_f/2-1$ coefficients per side are taken additionally.

Further, the effect of a smoothed output of the filter bank is studied. Therefore a nonlinear filter is applied at each detail level to reduce the influence of vanishing coefficients. The nonlinear smoothing filter is given by

$$(15)\qquad \begin{aligned} x_k &= \begin{cases} dx_{k-1} & \text{for} \quad u_k < dx_{k-1} \\ u_k & \text{for} \quad u_k \geq dx_{k-1} \end{cases} \\ y_k &= x_k. \end{aligned}$$

The filter is designed to quickly follow a positive change in the input value $u(k)$ while having a slow descent for temporary vanishing input values. Parameter d with $0 \leq d \leq 1$ controls the size of decline. In Fig. 8, the properties of the filter are visualised. An input value smaller than the internal state $x(k)$ is disregarded, while a greater value is immediately put through to the output $y(k)$. This allows to quickly follow an increase of the wavelet coefficients, while a single vanishing coefficient is suppressed. However, a permanent change from high coefficients to low coefficient is followed shortly, determined by the choice of parameter d.

The described wavelet coefficient sets VS and IP in combination with the filter are studied in application to NUA phase detection. Therefore a training data set is derived from measurements and SVMs are trained to detect the different operational phases *Idle* (c_1), *Transient* (c_2), *Moving* (c_3) and *Stall* (c_4), as well as the event *Spike* (c_5) of the NUA, as described in section 2. For each phase a training data set as well as an independent validation data set is created. Based on this, individual classifiers are trained on the first set and their integrity in correct classification is assessed on the second data set. The integrity I of a classifier is here defined as

$$(16)\qquad I = 1 - \alpha - \beta,$$

where α is the false positive rate (error type I) and β is the false negative rate (error type II). Both error types are here considered equally worse. The classifier is designed to have an integrity near or equal to one. Further it is judged by n_{SV}, which is the number of SVs, as this determines the computational complexity of the decision function.

The first experiment is used to find the appropriate number of decomposition levels of the wavelet filter bank. Here, the coefficient set VS is examined without application of a smoothing filter. The decomposition level n is increased, starting with $n = 3$, which results in different lengths of the feature vector $\mathbf{x}_\mathrm{w}$ with increasing information. The free parameters in SVM training are varied and for each level and class the SVM with best integrity is chosen as classifier. All SVMs have a Gaussian kernel function. In Tab. 1 the results of the this analysis are summarised. The integrity for the detection of class c_1 to c_4 rises with increasing decomposition level. Especially the detection of the phases *Transient* (c_2) and *Move* (c_3) are significantly improved by higher decomposition levels. All classes can be reliably detected for $n = 6$ where the integrity is above 99.6 % for each class. The number of SVs increases slightly with higher decomposition level. A decomposition level of $n = 6$ is assumed to be appropriate for NUA phase detection with SVC and is considered in the following.

TAB. 1: SVM integrity and (n_{SV}) by decomposition level

Class	Level n			
	3	4	5	6
c_1	0.9619 (10)	0.9973 (22)	1.0000 (37)	1.0000 (102)
c_2	0.6577 (37)	0.8607 (98)	0.9573 (94)	0.9979 (101)
c_3	0.8157 (17)	0.9367 (75)	0.9881 (65)	0.9961 (97)
c_4	0.9328 (20)	0.9963 (57)	0.9985 (39)	0.9992 (70)

TAB. 2: SVM integrity and (n_{SV}) by modifications at $n = 6$

Class	Vertical Slice		Impulse Pyramid	
	No Filter	Filter	No Filter	Filter
c_1	1.0000 (102)	1.0000 (64)	1.0000 (27)	1.0000 (14)
c_2	0.9979 (101)	1.0000 (29)	1.0000 (192)	1.0000 (96)
c_3	0.9961 (97)	1.0000 (17)	1.0000 (171)	0.9996 (84)
c_4	0.9992 (70)	0.9998 (23)	1.0000 (165)	1.0000 (96)
c_5	0.9660 (62)	0.9763 (77)	0.9935 (54)	0.9954 (38)

In the second experiment, the effect of the two modifications (smoothing filter and impulse pyramid configuration) is analysed to further improve the quality of the classifiers. In Tab. 2 the results are summarised. It shows that the smoothing filter improves the integrity and at the same time reduces the number of SVs significantly. The feature configuration IP mainly affects the integrity of the classifier for spike detection (c_5). Using both modifications together results in classifiers for classes c_1 to c_4 with an integrity greater than 99.9 % and for c_5 greater than 99.5 %. The number of SVs for each classifier is lower than 100.

The results show a considerable improvement while using the smoothing filter in combination with the impulse pyramid configuration for derivation of wavelet features. By using both modifications the significance of the wavelet features is enhanced, compared to using only the actual output of the filter bank. With these enhanced wavelet features the different phases of the NUA, as well as the spike events, can be detected with high reliability.

The designed SVMs are now applied for phase detection of the NUA by using the enhanced features. The phase detection is actually a multi-class-problem which can lead to an ambiguity in the detected phase. This can occur when two or more classifiers respond positive to a given pattern concurrently. To remove this ambiguity a consolidation step is used. The SVM classifier outputs either $+1$ denoting a pattern in its class or -1 otherwise. This digital output is low-pass filtered and the classifier with maximum filter output is considered to represent the consolidated phase estimate. Besides this, the SVM for spike detection is considered separately. The occurrence of spikes is independent of the actual NUA phase. In Fig. 9 the result of the NUA phase detection is shown for a system in a fault free state. The upper graph shows the measured input current signal of the NUA. As described above, wavelet features are taken from a six level wavelet filter bank. The plot of the discrete Wavelet transformation is shown in the middle graph. The bottom graph visualises the result after the phase detection by SV classifiers for c_1 to c_4, the phase estimation is mutually exclusive after the consolidation step. The spike detection c_5 is independent from the phase detection. The estimated phase closely follows the described behaviour in section 2. The NUA operation starts with a inrush transient which immediately changes to a rather stationary phase where the NUA moves constantly. Phase c_3 is properly detected. The second transient marks the end of the phase *Move* before going into the *Stall* phase. The beginning of the *Stall* phase is detected correctly, but the small number of spikes around 0.25 s causes the phase estimate to intermittently switch to the *Transient* phase. However, the spikes are detected by classifier c_5, the time of occurrence as well as the number of spikes can be determined.

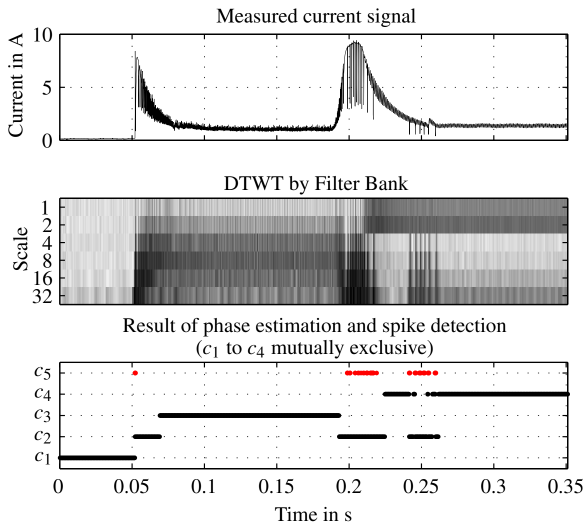

FIG. 9: Example of phase detection

5.2 State Detection

Phase and spike detection are used for the derivation of higher features describing the state of the NUA. This is discussed in the following section. The NUA system is assumed to be in either one of the three following states:

- State 1 (s_1) Normal Operation
- State 2 (s_2) Increased Friction
- State 3 (s_3) Degraded Motor

The first state describes the system in normal operation mode, while state 2 and 3 are fault states, as described in section 2. For the second state, the system has a increased internal friction, which is simulated by an applied side load. The third state represents a system with reduced motor efficiency by motor degradation simulated by the inclusion of a shunt resistor in one motor winding. A measurement series was taken which covers NUA operation in all three states. For both fault states the severity of the degrading factor was varied. In case of the induced friction the applied external load m_L is changed from 5 kg to 27 kg. For the induced motor degradation the shunt resistance R_S varies from $0.68\,\Omega$ to $5.6\,\Omega$. Based on the described phase detection and spike detection several higher features are derived:

- f_1 = Duration of phase *Move*
- f_2 = Duration of phase *Stall*
- f_3 = Duration of system being not-*Idle*
- f_4 = Duration from t_0 to begin of phase *Stall*
- f_5 = Dominant frequency in phase *Stall* (by STFT)
- f_6 = Number of detected spikes

For all 161 available measurement runs of NUA operation, the wavelet feature based phase detection is computed. Then, the higher features can be derived based on the information provided by the phase detection. Several higher features turned out to be either strongly correlated or not sensitive to the considered faults. However, the features f_4 and f_6 are not correlated and prove to be sensitive for fault states s_2 and s_3.

For state detection of the NUA two classifiers are needed, one to detect fault state s_2 and a second one to detect fault state s_3. A classifier for detection of the normal operation mode is not necessary as the system is assumed to be fully functional if none of the two fault states is present. Two nonlinear SVMs are trained to detect s_2 and s_3, both having a Gaussian kernel function. The obtained classifiers are visualised in Fig. 10. Based on the underlying training data set, the considered classes s_2 and $s_1 \cup s_3$ are fully separable. As the number of available data sets was small all data sets are used for SVM training, no separate validation set could be used. For applied loads greater than 5 kg the fault state 2 is separable from the rest, the integrity of the classifier is equal to 1. The second classifier is trained to detect state 3, here the considered classes s_3 and $s_1 \cup s_2$ are not fully separable. For larger shunt resistances the classes overlap. However, for shunt resistances smaller than $5.6\,\Omega$ the overlap is small, the obtained classifier results in a false negative rate of $\beta = 0.1154$. The false positive rate is zero, hence the integrity is found as $I = 0.8846$. For smaller shunt resistor values the detection of motor degradation is reliable.

5.3 Health Assessment

The aim of a succeeding health assessment step is to find a continuous measure of the system health compared to the so far digital state information provided by the state detection step. Therefore it is necessary to find a measure which is correlated with the effect causing the system degradation. In case of the NUA, a measure is needed to quantify the effect of increased internal friction and a second measure to quantify the motor degradation. Both features discussed in subsection 5.2 provide such a quantitative measure for the considered faults. It shows that f_4 is correlated with the internal friction. Higher values of this feature correspond

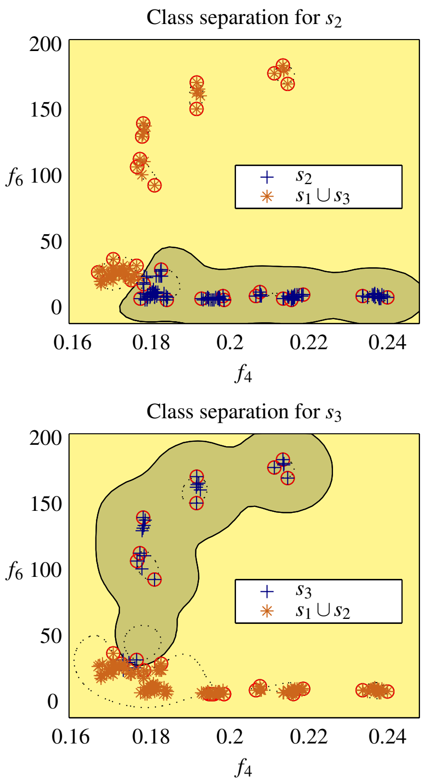

FIG. 10: Classifier for detection of states s_2 and s_3

with higher applied mechanical load i. e. induced friction. The features f_4 and f_6 together indicate a low shunt resistance and therefore an induced motor degradation.

The health assessment of the NUA is formed by two regression functions which are used to describe the relationship between the features and the degrading influence. With function h_1 the relation between (f_4, f_6) and m_L is approximated, and with h_2 the relation between f_4 and R_L. Both approximation functions

$$\hat{m}_L = h_1(f_4, f_6), \tag{17a}$$

$$\hat{R}_S = h_2(f_4), \tag{17b}$$

are assumed to be linear. The regression functions are computed by least squares. The estimation errors of both regression functions are given in Fig. 11. The approximation errors $e_m = m_L - \hat{m}_L$ for the estimated mass and the resulting boxplots, showing the error distributions, are given in the upper graph. Using the linear regression function, the approximation error is rather large for low load levels. However, it seems possible to correct the error as it has a large bias while the variance is small. For higher load levels the bias gets smaller. The fitted linear function is applicable for health assessment of the NUA to detect internal friction induced by a mechanical load. The second graph shows the errors for $e_R = R_S - \hat{R}_S$ of a linear regression. Again the absolute approximation errors are rather small, except for the third level at $2.7\,\Omega$, where a larger deviation is observed. However, the estimation errors are assumed to be acceptable for derivation of a NUA health assessment

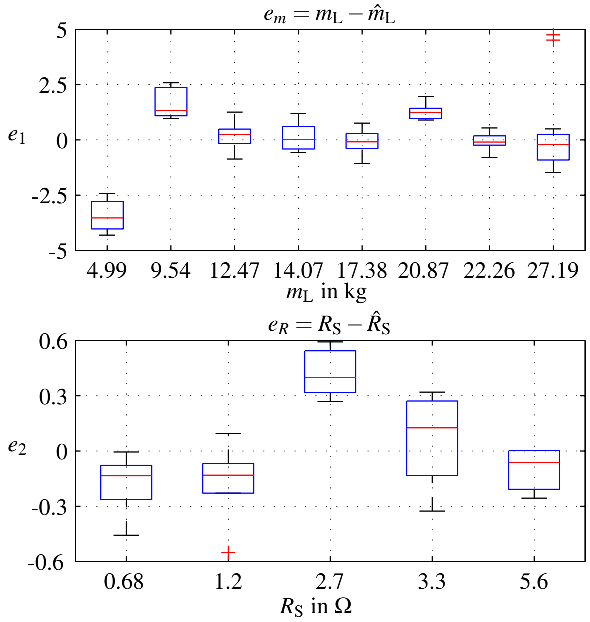

FIG. 11: Estimation errors of HA functions

index. The estimated values for load and shunt resistance can be used in a linear scaling function to map the values to interval [0,1] which is interpreted as a health index of the system.

This concludes the health assessment scheme for the NUA. Two independent faults can be detected and quantified regarding their severity. Further studies should address the following step in the OSA-CBM model which derives prognostic information about the remaining useful life of the system. To achieve this, reliable prognosis models for fault evolvement are needed to describe the fault progress after detection of an incipient fault. This requires either a fully understood fault mechanism to model its behaviour or meaningful observations taken from a set of systems under real service.

6 CONCLUSION

A health assessment scheme for the Normal Uplock Actuator is proposed in this work. The health assessment solely uses the motor input current signal which is already available on-board the aircraft. Further, the scheme uses only the system immanent excitation; no test signal is applied.

The current signal is analysed and meaningful features for reliable state detection are derived using wavelet features. Different configurations for the derivation of wavelet features are studied. The effect of a smoothing filter and the utilisation of adjacent coefficients have shown to improve the informational value of the features. These enhanced wavelet features are taken as input for a bank of Support Vector Machines for phase detection, which leads to derivation of higher features for NUA state detection. The considered system faults can be diagnosed reliable and further on their severity can be quantified. The feasibility of a health assessment step is shown by the estimation of the quantity which causes the system degradation.

Future work has to address the realisation of a fault prognosis step. This step is mandatory for the exploitation of the full capability of condition-based maintenance.

REFERENCES

[1] C.J.C. Burges. A Tutorial on Support Vector Machines for Pattern Recognition. *Data Mining and Knowledge Discovery*, 2(2), 1998.

[2] L. Cohen. *Time-Frequency Analysis*. Prentice-Hall, 1995.

[3] I. Daubechies. *Ten Lectures on Wavelets*. SIAM: Society for Industrial and Applied Mathematics, 1992.

[4] S. Mallat. *A Wavelet Tour of Signal Processing*. Academic Press, 1999.

[5] S. G. Mallat. A Theory for Multiresolution Signal Decomposition: The Wavelet Representation. *IEEE Transactions on Patttern Analysis and Machine Intelligence*, 11(7), 1989.

[6] J. Schaab, M. Münchhof, and M. Vogt. Identification of a Hydraulic Servo-Axis using Support Vector Machines. In *Proc. 7. IFAC World Congress*, 2005.

[7] B. Schölkopf and A.J. Smola. *Learning with Kernels*. The MIT Press, Cambridge, MA, 2002.

[8] H.-G. Stark. *Wavelets and Signal Processing*. Springer-Verlag, 2005.

[9] G. Strang and T. Nguyen. *Wavelets and Filter Banks*. Wellesley-Cambridge Press, 1997.

[10] M. Thurston and M. Lebold. Open Standards for Condition-Based Maintenance and Prognostic Systems. *MARCON*, 2001. www.osacbm.org, www.mimosa.org.

[11] V. N. Vapnik. *The Nature of Statistical Learning Theory*. Springer-Verlag, New York, 1995.